Laser Interferometric Gravitational-Wave Observatory (LIGO)

Measuring space-strains to "smaller than one part in 10^{21}"
and
All about "shot noise"

References

- http://www.ligo.caltech.edu
- http://www.ligo.org/science/overview.php
- "LIGO…", Rep. Prog. Phys. **72** (2009)
- "Recycling in LIGO detectors," Phys. Rev. D (1999).
- "GW beyond the quantum shot-noise limit," Nature-Phys. **7** (2011)

Gravity Waves

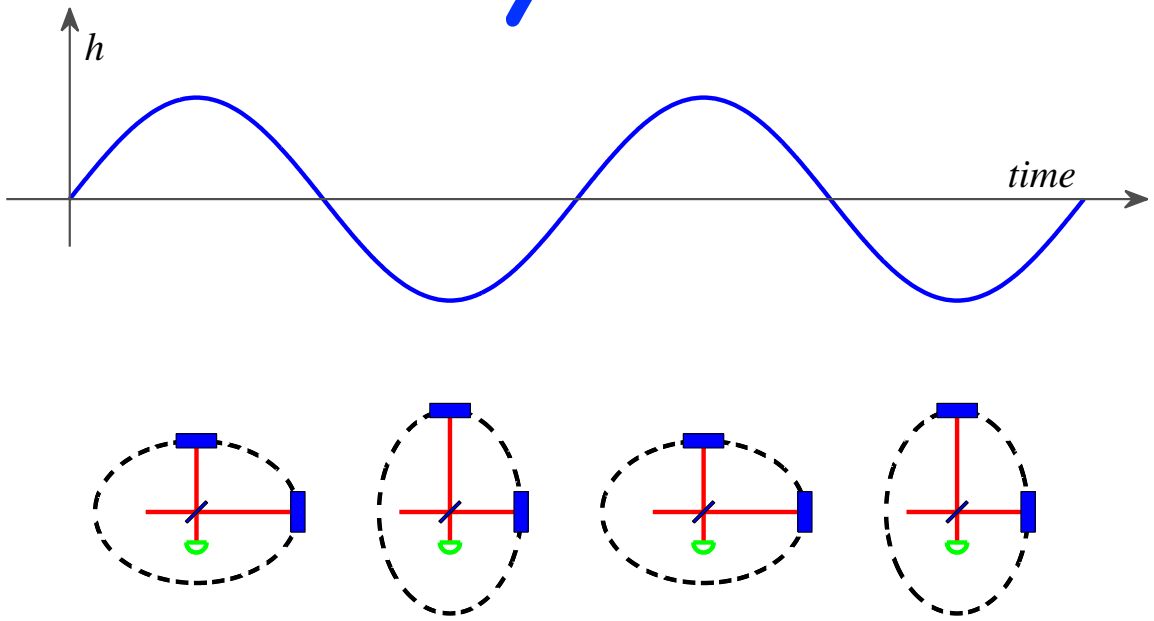

Figure 1. A GW traveling perpendicular to the plane of the diagram is characterized by a strain amplitude h. The wave distorts a ring of test particles into an ellipse, elongated in one direction in one half-cycle of the wave, and elongated in the orthogonal direction in the next half-cycle. This oscillating distortion can be measured with a Michelson interferometer oriented as shown. The length oscillations modulate the phase shifts accrued by the light in each arm, which are in turn observed as light intensity modulations at the photodetector (green semi-circle). This depicts one of the linear polarization modes of the GW.

LIGO Interferometers

Table 1. Parameters of the LIGO interferometers. H1 and H2 refer to the interferometers at Hanford, Washington, and L1 is the interferometer at Livingston Parish, Louisiana.

	H1	L1	H2
Laser type and wavelength		Nd : YAG, $\lambda = 1064$ nm	
Arm cavity finesse		220	
Arm length (m)	3995	3995	2009
Arm cavity storage time, τ_s (ms)	0.95	0.95	0.475
Input power at recycling mirror (W)	4.5	4.5	2.0
Power Recycling gain	60	45	70
Arm cavity stored power (kW)	20	15	10
Test mass size and mass		$\varnothing 25$ cm $\times$ 10 cm, 10.7 kg	
Beam radius ($1/e^2$ power) ITM/ETM	3.6 cm/4.5 cm	3.9 cm/4.5 cm	3.3 cm/3.5 cm
Test mass pendulum frequency (Hz)		0.76	

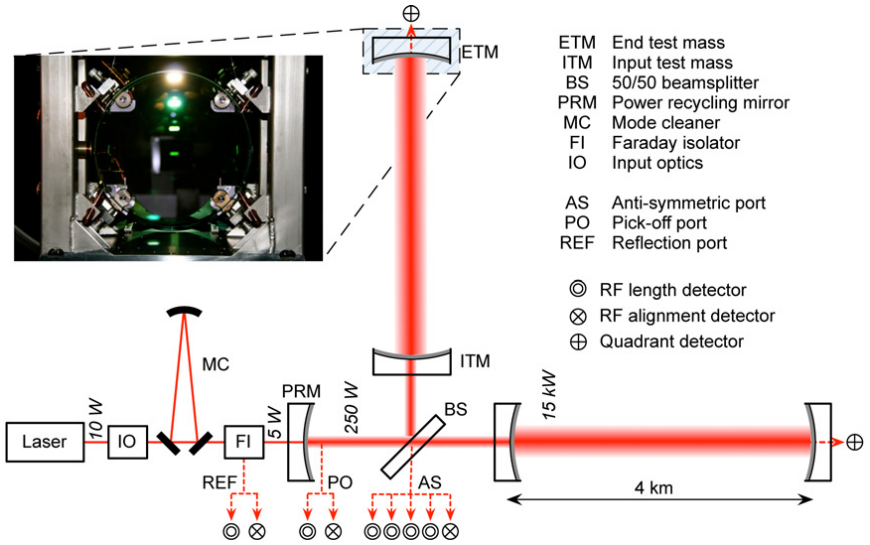

Figure 3. Optical and sensing configuration of the LIGO 4 km interferometers (the laser power numbers here are generic; specific power levels are given in table 1). The IO block includes laser frequency and amplitude stabilization, and electro-optic phase modulators. The power recycling cavity is formed between the PRM and the two ITMs, and contains the BS. The inset photo shows an input test mass mirror in its pendulum suspension. The near face has a highly reflective coating for the infrared laser light, but transmits visible light. Through it one can see mirror actuators arranged in a square pattern near the mirror perimeter.

The Nobel Prize in Physics 1993
Russell A. Hulse, Joseph H. Taylor Jr.

Russell A. Hulse

Joseph H. Taylor Jr.

The Nobel Prize in Physics 1993 was awarded jointly to Russell A. Hulse and Joseph H. Taylor Jr. *"for the discovery of a new type of pulsar, a discovery that has opened up new possibilities for the study of gravitation"*

Demonstration of gravitational waves

A very important observation was made when the system had been followed for some years. This followed theoretical predictions made shortly after the original discovery of the pulsar. It was found that the orbit period is declining: the two astronomical bodies are rotating faster and faster about each other in an increasingly tight orbit. The change is very small. It corresponds to a reduction of the orbit period by about 75 millionths of a second per year, but, through observation over sufficient time, it is nevertheless fully measurable. This change was presumed to occur because the system is emitting energy in the form of gravitational waves in accordance with what Einstein in 1916 predicted should happen to masses moving relatively to each other. According to the latest data, the theoretically calculated value from the relativity theory agrees to within about one half of a percent with the observed value. The first report of this effect was made by Taylor and co-workers at the end of 1978, four years after the discovery of the binary pulsar was reported.

The good agreement between the observed value and the theoretically calculated value of the orbital path can be seen as an indirect proof of the existence of gravitational waves. **We will probably have to wait until next century for a direct demonstration of their existence.** Many long-term projects have been started for making direct observations of gravitational waves impinging upon the earth. The radiation emitted by the binary pulsar is too weak to be observed on the earth with existing techniques. However, perhaps the violent perturbations of matter that take place when the two astronomical bodies in a binary star (or a binary pulsar) approach each other so closely that they fall into each other may give rise to gravitational waves that could be observed here.

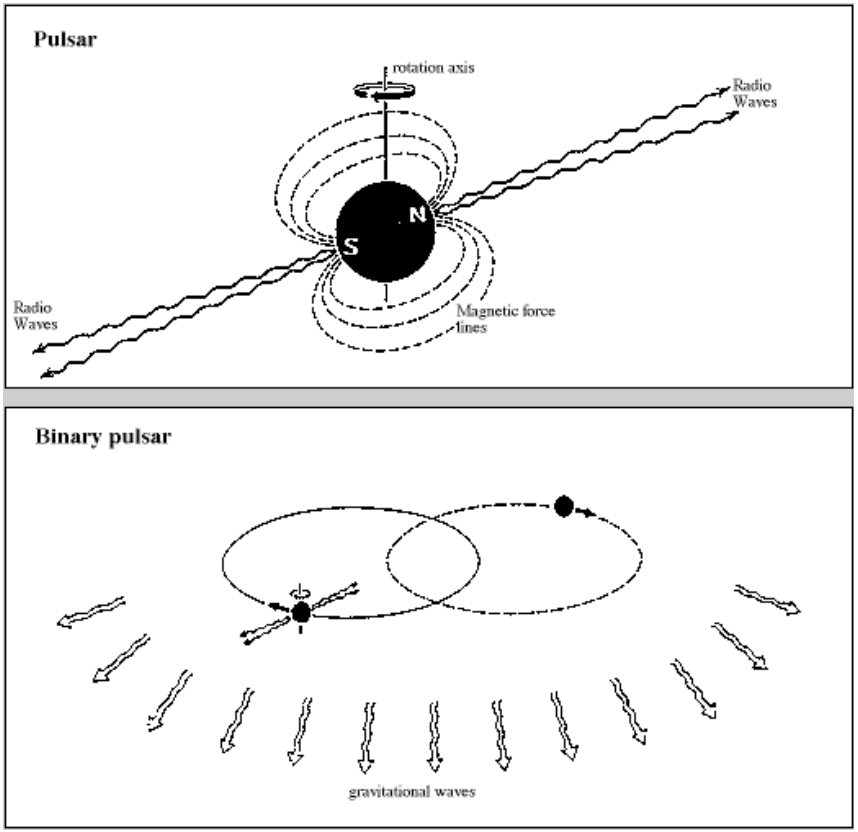

The radio waves from a pulsar are emitted in two bunches which sweep across space at the same rate as the pulsar rotates (upper figure). From a binary pulsar, gravitational waves are also emitted (lower figure).

Noise

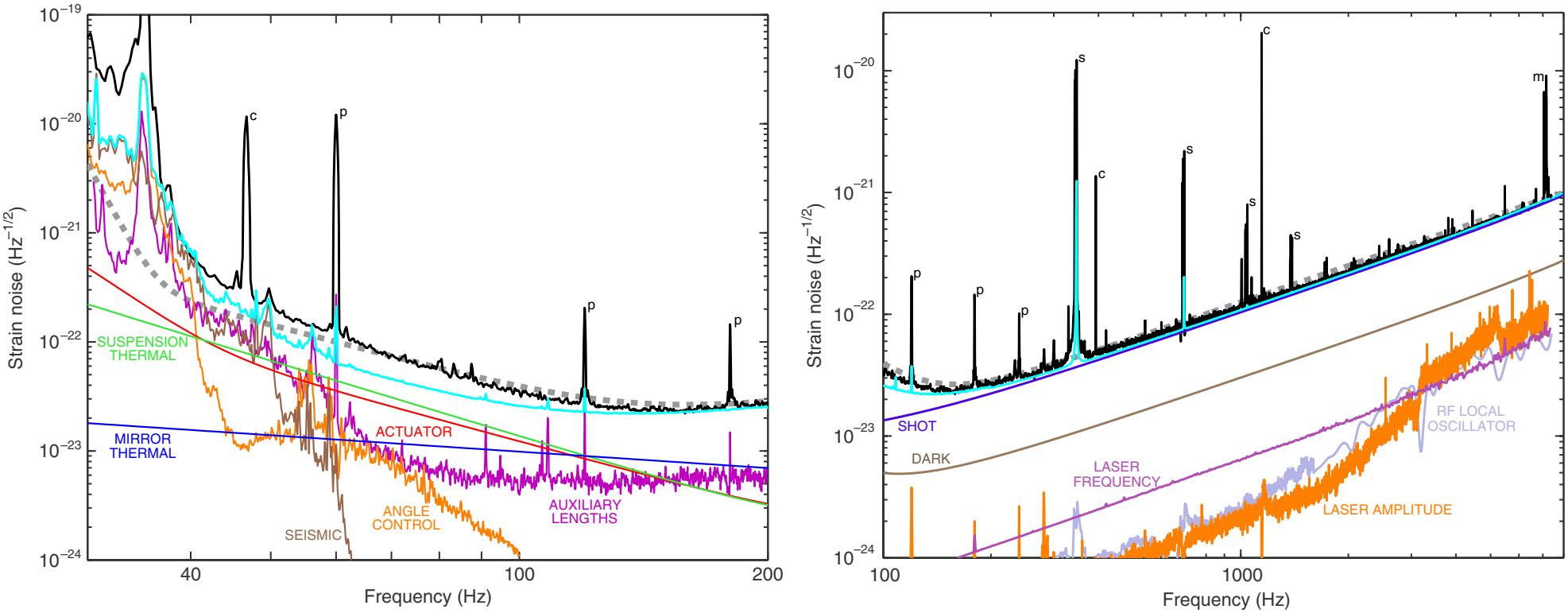

Figure 7. Primary known contributors to the H1 detector noise spectrum. The upper panel shows the displacement noise components, while the lower panel shows sensing noises (note the different frequency scales). In both panels, the black curve is the measured strain noise (same spectrum as in figure 6), the dashed gray curve is the design goal and the cyan curve is the root-square-sum of all known contributors (both sensing and displacement noises). The labeled component curves are described in the text. The known noise sources explain the observed noise very well at frequencies above 150 Hz, and to within a factor of 2 in the 40–100 Hz band. Spectral peaks are identified as follows: c, calibration line; p, power line harmonic; s, suspension wire vibrational mode; m, mirror (test mass) vibrational mode.

Shot Noise: Dominant Sensing Noise

- How many photons?
- What is cavity storage time?
- What is AS detected power?
- ...as a function of strain?
- What is strain noise?
- ...as a function of GW frequency, f?

5.2. Sensing noise sources

Sensing noises are shown in the lower panel of figure 7. By design, the dominant noise source above 100 Hz is shot noise, as determined by the Poisson statistics of photon detection. The ideal shot-noise limited strain noise density, $\tilde{h}(f)$, for this type of interferometer is [9]

$$\widetilde{h}(f) = \sqrt{\frac{\pi\hbar\lambda}{\eta P_{\mathrm{BS}} c}} \frac{\sqrt{1+(4\pi f\tau_{\mathrm{s}})^2}}{4\pi\tau_{\mathrm{s}}}, \tag{2}$$

where λ is the laser wavelength, $\hbar$ is the reduced Planck constant, c is the speed of light, τ_{s} is the arm cavity storage time, f is the GW frequency, P_{BS} is the power incident on the beamsplitter and η is the photodetector quantum efficiency. For the estimated effective power of $\eta P_{\mathrm{BS}} = 0.9 \times 250\,\mathrm{W}$, the ideal shot-noise limit is $\tilde{h} = 1.0 \times 10^{-23}\,\mathrm{Hz}^{-1/2}$ at 100 Hz. The shot-noise estimate in figure 7 is based on measured photocurrents in the AS port detectors and the measured interferometer response. The resulting estimate, $\tilde{h}(100\,\mathrm{Hz}) = 1.3 \times 10^{-23}\,\mathrm{Hz}^{-1/2}$, is higher than the ideal limit due to several inefficiencies in the heterodyne detection process: imperfect interference at the beamsplitter increases the shot noise; imperfect modal overlap between the carrier and RF sideband fields decreases the signal and the fact that the AS port power is modulated at twice the RF phase modulation frequency leads to an increase in the time-averaged shot noise [39].

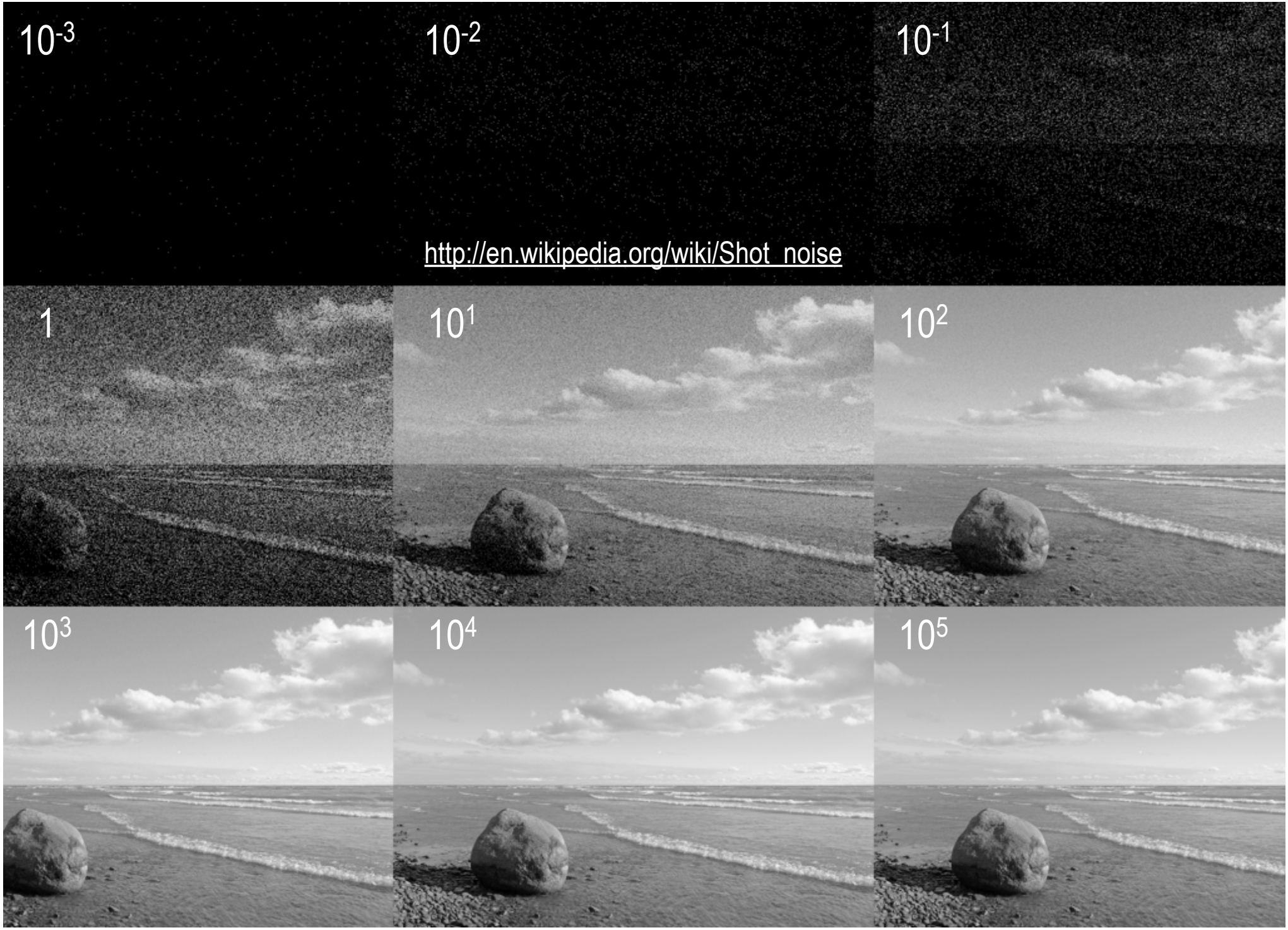
10^{-3}
10^{-2}
10^{-1}
http://en.wikipedia.org/wiki/Shot_noise
1
10^{1}
10^{2}
10^{3}
10^{4}
10^{5}

Shot-Noise: a Poisson Process

- δN = ±√N (i.e. variance = N)
- (photons/sec)
  ⟨N⟩ per second = $P/\hbar\omega = P\lambda/2\pi\hbar c$
- Within an interval Δt = 1/2Δf, ...

$$\delta P = \pm \hbar\omega\sqrt{N}/\Delta t = \pm\sqrt{2\hbar\omega P\Delta f}$$

Next Week:
Refrigerating Phonons